Journal of Sound and Vibration (1999) **222**(1), 115–143
Article No. jsvi.1998.2040, available online at http://www.idealibrary.com on IDEAL

ACOUSTIC BESSEL BULLETS

P. R. STEPANISHEN
Department of Ocean Engineering, University of Rhode Island, Narragansett, RI 02882, *U.S.A.*

(*Received* 23 *March* 1998, *and in final form* 5 *November* 1998)

Acoustic Bessel Bullets (BB) are defined to be a new class of band-limited Transient Bessel Beams or localized waves which maintain their shape and amplitude as they propagate in space. The space–time properties of acoustic BB fields generated by planar spatial apertures excited with gated sinusoidal excitations are investigated using a recently developed generalized impulse response approach. Analytical results are presented for the general characteristics of acoustic BB fields generated by infinite and finite planar apertures as a function of center excitation frequency and bandwidth. Numerical results are then presented to illustrate the space–time properties of the on-axis field for acoustic BB fields relative to those of a conventional piston source. The near to farfield transition distance for acoustic BB fields is investigated and compared to the Rayleigh distance for a piston source. Important edge wave effects and anomalous spatial decay rates are observed and discussed.

1. INTRODUCTION

In 1983, Brittingham discovered the first localized wave (LW) solution to the homogeneous Maxwell's equation which he termed the Focus Wave Mode (FWM) [1]. A free parameter in the solution determines the overall characteristics of the field corresponding to a quasi transverse plane wave at one extreme and a narrow spatially transverse pulse at the other extreme. Ziolkowski subsequently used the FWM solution as a kernel for constructing new localized wave (LW) solutions [2]. In particular, the Modified Power Spectrum (MPS) pulse developed by Ziolkowski has received enormous attention in the literature [3–11].

In two recent papers [12, 13], Stepanishen developed a new class of localized waves which maintain their shape and amplitude as they propagate in space. These localized waves were designated as acoustic bullets or acoustic Transient Bessel Beams (TBB). In contrast to the FWM and MPS solutions a TBB field maintains its temporal and spatial shape as the acoustic bullet propagates in free space from an infinite planar aperture. The three dimensional TBB field thus exhibits the same characteristic as the D'Alembert solution [14] to the one-

0022–460X/99/160115 + 29 $30.00/0

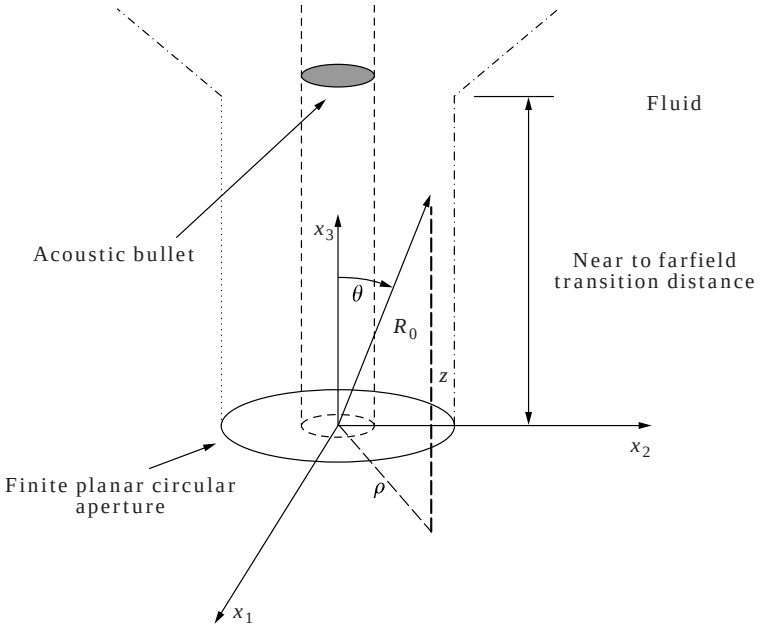

Figure 1. A finite planar circular aperture.

dimensional wave equation, i.e., the waves exhibit no change in shape about the pulse center as they propagate.

Although the exact TBB solution in all space can not be generated from a finite planar aperture, the general characteristics of TBB fields can be realized in a limited space–time region. In particular, an acoustic bullet with a smaller support region than the circular aperture can be launched from a finite aperture [12] as illustrated in Figure 1. In the nearfield region the field exhibits properties similar to those observed for the infinite aperture case, and in the farfield region the field exhibits an inverse range dependence. It is of interest to note that the lateral extent of the acoustic bullet may be smaller than the aperture.

A generalized impulse response approach to investigate the on-axis and farfield space–time properties of TBB fields was developed in a recent paper [13]. This approach is an extension of a previously developed impulse response approach [14] to investigate the space–time properties of fields which are generated by pistons, i.e., sources with uniform velocity distributions. Important characteristics of the space–time impulse responses associated with general TBB fields were presented in the recent paper; however, no numerical results for TBB fields, which can be realized in practice, were presented.

The space–time properties of the acoustic field for a particular class of acoustic bullet or TBB field which is designated here as an acoustic Bessel Bullet (BB) is investigated in the present paper. These wave fields are associated with gated sinusoidal signals. In contrast to previously addressed [12, 13] baseband signals of interest, an acoustic BB has a bandpass frequency spectrum and is

thus more readily generated from typical planar piezoelectric transducers which naturally exhibit bandpass filter characteristics. A brief review of the general theory for acoustic bullet or TBB field is first presented in section 2, acoustic BB fields are defined in section 3.

Analytical results for the space–time on-axis field and farfield properties of acoustic BB fields are developed in section 3, for infinite and finite planar apertures using the recently developed generalized impulse response approach [13]. Estimates are first presented for the axial and lateral resolution for acoustic BB fields which are generated by infinite planar apertures. Estimates of the near to farfield transition range for acoustic BB fields which are generated by finite planar apertures are then developed via the impulse response approach.

Numerical results for the case of an infinite aperture are presented in section 4 to illustrate the effects of carrier frequency and pulse length on the axial and lateral extent and the general space–time properties of acoustic BB fields. Numerical results for the case of a finite aperture are then presented to illustrate the general space–time properties of the on-axis field for acoustic BBs relative to the field generated from the aperture with a spatially uniform excitation. These results clearly indicate the importance of the edge generated wave on the beam formation process. In addition, an interesting anomalous on-axis far field decay rate is observed for selected frequencies.

2. GENERAL THEORY

The acoustic wave equation for the axisymmetric pressure fields of interest $p(\rho, z, \tau)$ can be expressed in the normalized cylindrical co-ordinate system illustrated in Figure 1 as

$$\left[\frac{1}{\rho}\frac{\partial}{\partial\rho}\left(\rho\frac{\partial}{\partial\rho}\right)+\frac{\partial^2}{\partial z^2}-\frac{\partial^2}{\partial\tau^2}\right]p(\rho, \varphi, z, \tau)=0, \tag{1}$$

where (ρ, z) are the normalized spatial co-ordinates and the normalized time is $\tau = c_0 t/L$, where t denotes the unscaled time variable, c_0 is the constant sound speed of the media, and L is a characteristic length for the planar aperture of interest. It has been recently shown [12] that general TBB fields which exhibit the properties of acoustic bullets in an unbounded free space can be expressed as

$$p(\rho, z, \tau) = w(\tau) \otimes j(\rho, z, \tau), \tag{2}$$

where $w(\tau)$ is an arbitrary weighting function which can be used to control the spectral properties of the field, $\otimes$ denotes the convolution operator and

$$j(\rho, z, \tau) = \frac{1}{\pi[(\rho\sin\zeta)^2-(\tau - z\cos\zeta)^2]^{1/2}}, \quad -\rho\sin\zeta + z\cos\zeta < \tau < \rho\sin\zeta + z\cos\zeta. \tag{3}$$

For the on-axis case where $\rho = 0$ it is noted that

$$j(0, z, \tau) = \delta(\tau - z\cos\zeta) \tag{4}$$

and the sifting property of the Dirac delta function $\delta(\ )$ then leads to the result

$$p(0, z, \tau) = w(\tau - z\cos\zeta). \tag{5}$$

Stepanishen [13] has recently shown that the TBB field generated from a finite planar aperture as illustrated in Figure 1 can be expressed as

$$p(\rho, z, \tau) = \frac{\mathrm{d}w(\tau)}{\mathrm{d}\tau} \otimes h_\sigma(\rho, z, \tau) \tag{6}$$

$$= w(\tau) \otimes \frac{\mathrm{d}h_\sigma(\rho, z, \tau)}{\mathrm{d}\tau}, \tag{7}$$

where the generalized space–time impulse response $h_o(\rho, z, \tau)$ is defined as

$$h_\sigma(\rho, z, \tau) = \cos\zeta \int_0^\sigma \rho_s \,\mathrm{d}\rho_s \int_0^{2\pi} \mathrm{d}\phi_s \frac{1}{2\pi R}\; j(\rho_s, 0, \tau_s)_{\tau_s = r - R}. \tag{8}$$

R is the distance between a point on the aperture and the spatial point of interest and σ is the (normalized) radius of the aperture. Relatively simple closed form expressions, which are repeated below for convenience, and associated numerical results for the on-axis and farfield generalized space–time impulse response were presented in the earlier paper.

For the on-axis case where $0 \leqslant z/z_t < 1$, $h_\sigma(0, z, \tau)$ can be expressed in the simple form

$$h_\sigma(0, z, \tau) = u(\tau - z\cos\zeta) - u(\tau - \sqrt{\sigma^2 + z^2} + \sigma\sin\zeta) + d_\sigma(0, z, \tau), \tag{9}$$

where $u(\ )$ denotes the Heaviside function, the transition distance $z_t = \sigma/\tan\zeta$ and

$$d_\sigma(0, z, \tau) = -\frac{1}{\pi}\left\{\sin^{-1}\left[\frac{\tau - r_\sigma\cos^2\zeta}{\sin\zeta\sqrt{\tau^2 - z^2\cos^2\zeta}}\right] - \sin^{-1}\left[\frac{\tau - r_2\cos^2\zeta}{\sin\zeta\sqrt{\tau^2 - z^2\cos^2\zeta}}\right]\right\} \tag{10}$$

with $\sqrt{\sigma^2+z^2} - \sigma\sin\zeta < \tau < \sqrt{\sigma^2+z^2} + \sigma\sin\zeta$. Additionally, $r_\sigma = \sqrt{\sigma^2+z^2}$, $r_1 = \sqrt{\rho_1^2+z^2}$ and

$$\rho_1 = \frac{-\tau\sin\zeta + \sqrt{\tau^2 - z^2\cos^2\zeta}}{\cos^2\zeta}. \tag{11}$$

For $z/z_t > 1$ it was also shown that

$$h_\sigma(0, z, \tau) = -\frac{1}{\pi}\left\{\sin^{-1}\left[\frac{\tau - r_\sigma\cos^2\zeta}{\sin\zeta\sqrt{\tau^2 - z^2\cos^2\zeta}}\right] - \sin^{-1}\left[\frac{\tau - r_1\cos^2\zeta}{\sin\zeta\sqrt{\tau^2 - z^2\cos^2\zeta}}\right]\right\},$$

for $\sqrt{\sigma^2 + z^2} - \sigma\sin\zeta < \tau < z$,

$$= -\frac{1}{\pi}\left\{\sin^{-1}\left[\frac{\tau - r_\sigma \cos^2\zeta}{\sin\zeta\sqrt{\tau^2 - z^2\cos^2\zeta}}\right] - \sin^{-1}\left[\frac{\tau - r_2\cos^2\zeta}{\sin\zeta\sqrt{\tau^2 - z^2\cos^2\zeta}}\right]\right\},$$

$$\text{for } z < \tau < \sqrt{\sigma^2 + z^2} + \sigma\sin\zeta, \tag{12}$$

where $r_1 = \sqrt{\rho_1^2 + z^2}$ with

$$\rho_1 = \frac{\tau\sin\zeta - \sqrt{\tau^2 - z^2\cos^2\zeta}}{\cos^2\zeta}. \tag{13}$$

and $r_2 = \sqrt{\rho_2^2 + z^2}$ with

$$\rho_2 = \frac{-\tau\sin\zeta + \sqrt{\tau^2 - z^2\cos^2\zeta}}{\cos^2\zeta}. \tag{14}$$

Finally, it was shown [13] that the farfield pressure can be simply expressed as

$$p_\sigma(\theta, \tau) = \frac{\mathrm{d}w(\tau)}{\mathrm{d}\tau} \otimes h_\sigma^f(\theta, \zeta, \tau), \tag{15}$$

where the farfield impulse response $h_\sigma^f(\theta, \zeta, \tau)$ is expressed as

$$h_\sigma^f(\theta, \zeta, \tau) = \frac{\sigma^2}{2R_0}\cos\zeta g_\sigma(\theta, \zeta, \tau - R_0) \tag{16}$$

and R_0 is defined in Figure 1. The impulse response $g_\sigma(\theta, \zeta, \tau)$ can be simply expressed in the form

$$g_\sigma(\theta, \zeta, \tau) = \frac{1}{[\sin^2\zeta - \sin^2\theta]}[\sin^2\zeta\, j(\sigma, 0, \tau) \otimes h_1(\zeta, \tau) - \sin^2\theta\hat{j}(\sigma, 0, \tau) \otimes h_1(\theta, \tau)], \tag{17}$$

where

$$\hat{j}(\sigma, 0, \tau) = j(\sigma, 0, \tau)|_{\zeta=\theta} \tag{18}$$

and

$$\begin{aligned} h_1(\zeta, \tau) &= \frac{1}{\pi\sigma\sin\zeta}\left[1 - \left(\frac{\tau}{\sigma\sin\zeta}\right)^2\right]^{1/2} \left|\frac{\tau}{\sigma\sin\zeta}\right| < 1 \\ &= 0 \left|\frac{\tau}{\sigma\sin\ \zeta}\right| < 1. \end{aligned} \tag{19}$$

3. ACOUSTIC BESSEL BULLETS

Consider now a special type of acoustic BB which is defined by the following gated sinusoidal weighting function $w(\tau)$

$$w(\tau) = w_0 \sin(\Omega_b \tau), \quad 0 \leqslant |\tau| \leqslant T = 2\pi N/\Omega_b, \tag{20}$$

where Ω_b and $2T$ are the frequency and pulse duration. It is noted that $w(\tau)$ is an odd non-causal time function which consists of $2N$ sinusoidal cycles. After defining the Fourier transform pair, i.e., $w(\tau) \Leftrightarrow W(\Omega)$, where

$$w(\tau) = \frac{1}{2\pi}\int_{-\infty}^{\infty} W(\Omega)\, e^{i\Omega\tau}\, d\Omega, \quad W(\Omega) = \int_{-\infty}^{\infty} w(\tau)\, e^{-i\Omega\tau}\, d\Omega, \tag{21, 22}$$

the Fourier transform of $w(\tau)$ is simply expressed as

$$\begin{aligned} W(\Omega) &= jw_0 T\left\{\frac{\sin[(\Omega_b + \Omega)T)]}{[(\Omega_b + \Omega)T)]} - \frac{\sin[(\Omega_b - \Omega)T)]}{[(\Omega_b - \Omega)T)]}\right\} \\ &= j\frac{2\pi N}{\Omega_b} w_0 \left\{\frac{\sin[2\pi N(1 + \Omega/\Omega_b)]}{[2\pi N(1 + \Omega/\Omega_b)]} - \frac{\sin[2\pi N(1 - \Omega/\Omega_b)]}{[2\pi N(1 - \Omega/\Omega_b)]}\right\}. \end{aligned} \tag{23}$$

The magnitude of $W(\Omega)/w_0 T$ versus the normalized frequency Ω/Ω_b is shown in Figure 2 for $N = 1$, 2 and 4. It is clearly observed from the results in Figure 2 that the relative bandwidth of the signal decreases as N increases and $w(\tau)$ is thus a quasi bandpass signal.

The space–time properties of the acoustic BB fields generated by infinite planar apertures based on the above weighting function are first investigated. The pressure field in the half space $z > 0$ is thus simply defined by equation (2). In light of the form of $j(\rho, z, \tau)$ in equation (3) it is apparent that the pressure field in the half space $z \geqslant 0$ can be simply expressed as

$$p(\rho, z, \tau) = p(\rho, 0, \tau - z\cos\zeta). \tag{24}$$

It is thus apparent that $p(\rho', 0, \tau)$ is a time limited non-causal odd function with a time duration equivalent to $2T + 2\rho' \sin\zeta$ which is propagated in the z direction with the supersonic velocity $1/\cos\zeta$.

Since $p(\rho, 0, \tau)$ may be simply used to define the entire field it is noted from equation (24) that $p(\rho, 0, \tau)$ can be expressed as

$$p(\rho, 0, \tau) = \int_{-\rho\sin\zeta}^{\rho\sin\zeta} \frac{w(\tau - \tau')}{\pi[(\rho\sin\zeta)^2 - (\tau')^2]^{1/2}}\, d\tau'. \tag{25}$$

It is easily shown that $p(\rho, 0, \tau)$ is an odd function of τ for all ρ and the on-axis pressure is simply expressed as follows for $w_0 = 1$:

$$p(0, 0, \tau) = \sin(\Omega_b \tau), \quad 0 \leqslant |\tau| \leqslant T = 2\pi N/\Omega_b. \tag{26}$$

Since $w(\tau)$ is a time limited function it is noted that the integrand in equation (25) may be zero over a portion of the interval of integration for various τ. For the special case where $(T - \rho\sin\zeta) > \pi/\Omega_b$, the preceding statement leads to the observation that $p(\rho, 0, \tau)$ can be decomposed into three terms: a turn-on

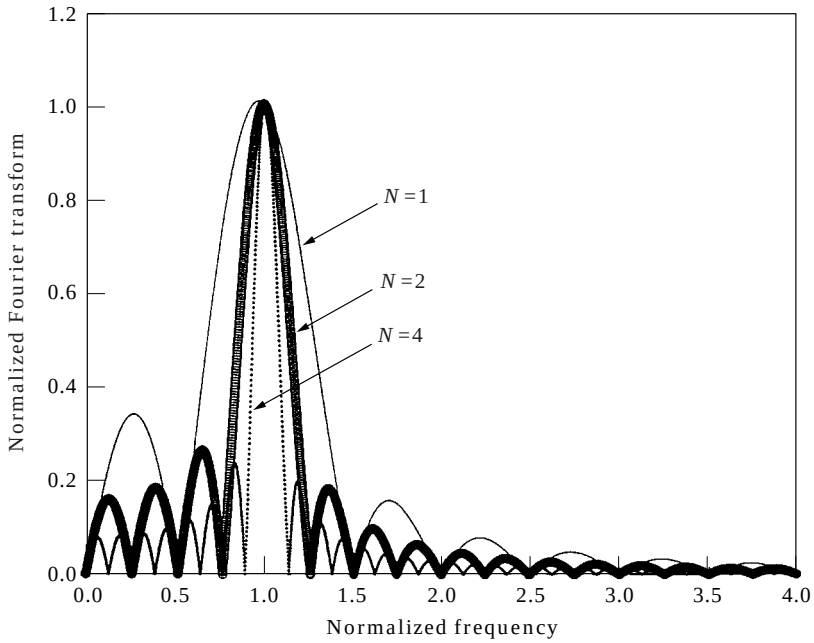

Figure 2. Normalized magnitude of $W(\Omega)$ versus normalized frequency Ω/Ω_b for $N = 1$, 2 and 4.

transient extending from $-(T + \rho \sin \zeta) < \tau < -(T - \rho \sin \zeta)$, a quasi steady state extending from $-(T - \rho \sin \zeta) < \tau < (T - \rho \sin \zeta)$, and a turn-off transient extending from $(T - \rho \sin \zeta) < \tau < (T + \rho \sin \zeta)$.

For $\rho \sin \zeta < T$, the quasi steady state pressure can now be simply described by the expression

$$p(\rho, 0, \tau) = \int_{-\rho \sin \zeta}^{\rho \sin \zeta} \frac{w(\tau - x^1)}{\pi[(\rho \sin \zeta)^2 - (\tau')^2]^{1/2}} \, d\tau'$$
$$= \int_{-1}^{1} \frac{w(\tau - \rho \sin \zeta y)}{\pi(1 - y^2)^{1/2}} \, dy \tag{27}$$

for $|\tau| \leqslant T - \rho \sin \zeta$. Since

$$w(\tau - \rho \sin \zeta y) = \sin(\Omega_b \tau) \cos(\Omega_b \rho \sin \zeta y) - \cos(\Omega_b \tau) \sin(\Omega_b \rho \sin \zeta y) \tag{28}$$

it then follows from the symmetry of the resultant integrands in equation (27) that $p(\rho, 0, \tau)$ can be expressed as

$$p(\rho, 0, \tau) = p_c(\Omega_b \rho \sin \zeta) \sin(\Omega_b \tau), \tag{29}$$

where

$$p_c(\Omega_b \rho \sin \zeta) = \int_{-1}^{1} \frac{\cos(\Omega_b \rho \sin \zeta y)}{\pi(1 - y^2)^{1/2}} \, dy = J_0(\Omega_b \rho \sin \zeta). \tag{30}$$

It is thus apparent that $p(\rho, 0, \tau)$ may only consist of a turn-on and turn-off transient at the radial distances ρ_m, where $J_0(\Omega_b \rho_m \sin \zeta) = 0$.

The lateral extent of the BB defined by the weighting function in equation (20) may now be readily estimated for the preceding case and conditions via the use of the quasi steady state pressure

$$p(\rho, 0, \tau) = J_0(\Omega_b \rho \sin \zeta) \sin(\Omega_b \tau), \tag{31}$$

which is also obviously valid for $\rho = 0$. If the lateral extent of the BB is defined by the radial location ρ_n where the quasi steady state field is reduced to $1/\sqrt{2}$ of the peak on-axis field, it is then apparent that

$$\rho_n \approx \frac{1}{\Omega_b \sin \zeta}. \tag{32}$$

Clearly, the lateral extent of the BB can then be simply controlled via the carrier frequency Ω_b of the weighting function whereas the on-axis axial extent of the BB, i.e., $2T$, is also a function of N. Thus, the lateral and axial extent of the BB can be independently controlled via the selection of Ω_b and N.

The space–time properties of the acoustic BB fields generated by a finite planar aperture based on $\sigma = 1$ and the weighting function in equation (20) are now investigated. In light of equations (9) and (6) the on-axis pressure field in the region $0 \leqslant z/z_t < 1$ can be simply expressed as

$$p_\sigma(0, z, \tau) = w(\tau - z \cos \zeta) + e(0, z, \tau), \tag{33}$$

where

$$e(0, z, \tau) = -w(\tau - \sqrt{1 + z^2} + \sin \zeta) + \frac{\mathrm{d}w(\tau)}{\mathrm{d}\tau} \otimes d_\sigma(0, z, \tau). \tag{34}$$

It is apparent that the initial term in equation (33) is the same as the result for the infinite aperture whereas $e(0, z, \tau)$ is a time limited edge wave which is non-zero over the time interval $\sqrt{1 + z^2} - \sin \zeta - T < \tau < \sqrt{1 + z^2} + \sin \zeta + T$. It is also noted that the on-axis pressure field in the region $1 \leqslant z/z_t$ can be simply expressed as

$$p_\sigma(0, z, \tau) = \frac{\mathrm{d}w(\tau)}{\mathrm{d}\tau} \otimes h_\sigma(0, z, \tau), \tag{35}$$

where $h_\sigma(0, z, \tau)$ is now specified by equation (12).

Several general observations regarding the on-axis field are now noted. It readily follows from the results in equations (9) to (12) that the impulse response $h_\sigma(0, z, \tau)$ exhibits different forms in different regions of the (z, τ) plane as illustrated in Figure 3, e.g., the impulse response is zero for $\tau < z \cos \zeta$ and $\tau > \sqrt{1 + z^2} + \sin \zeta$. In light of equations (33) and (34) it is also obvious that two separate non-overlapping pulses can occur in the region $0 \leqslant z < z_b < z_t$ if the pulse duration $2T < 1 - \sin \zeta$ is small enough. For this case in a space–time region bounded by z_b the edge wave does not overlap the initial pulse corresponding to the wave generated from an infinite aperture. The on-axis field

is thus the same as the field from the infinite aperture over a limited time window which decreases as z increases within $[0, z_b]$.

It is apparent from Figure 3 and the preceding discussion that the edge generated field and the initial field component associated with the infinite aperture field in the region $0 \leqslant z < z_t$ are separated in time by $\Delta\tau$, where

$$\Delta\tau = \sqrt{1+z^2} - \sin\zeta - z\cos\zeta. \tag{36}$$

The transition distance $z_t = \cot\zeta$ is noted to correspond to $\Delta\tau = 0$. For the case of a weighting function with a short pulse duration $2T$, it is apparent that two separate pulses will thus be observed over the range $[0, z_b]$ where $\sqrt{1+z_b^2} - \sin\zeta - z_b\cos\zeta = 2T$. Since the temporal separation decreases as z increases, it is clear from Figure 3 that z_b, the axial boundary of interest, is a monotonically decreasing function of T which is a maximum (z_t) for $2T \to 0$ and a minimum (0) for $2T = 1 - \sin\zeta$.

More generally, it is easily shown that $0 \leqslant z_b < z_t$ and z_b/z_t can be expressed as follows for $\zeta \neq 0$:

$$\begin{aligned} z_b/z_t &= 1 + \frac{2T}{\sin\zeta} - \frac{\sqrt{2\dfrac{2T}{\sin\zeta} + \left(\dfrac{2T}{\sin\zeta}\right)^2}}{2\cos\zeta}, \quad 2T < 1 - \sin\zeta \\ &= 0, \quad 2T > 1 - \sin\zeta. \end{aligned} \tag{37}$$

For the ζ range where $\cos\zeta \simeq 1$ it then follows that z_b/z_t can be expressed as a function of a single parameter $2T/\zeta$ for $\zeta \neq 0$, i.e.,

$$z_b/z_t = 1 + \frac{2T}{\zeta} - \frac{1}{2}\sqrt{2\frac{2T}{\zeta} + \left(\frac{2T}{\zeta}\right)^2}, \quad 2T < 1 - \zeta. \tag{38}$$

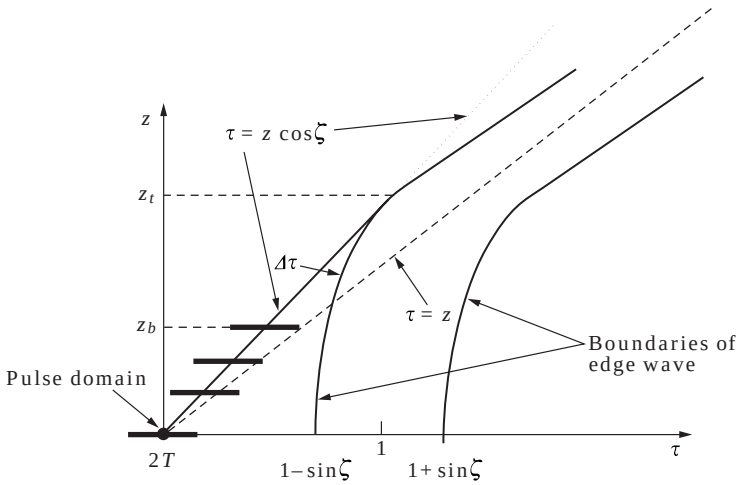

Figure 3. Space–time boundaries of the impulse response in the $\tau - z$ plane and the spatial

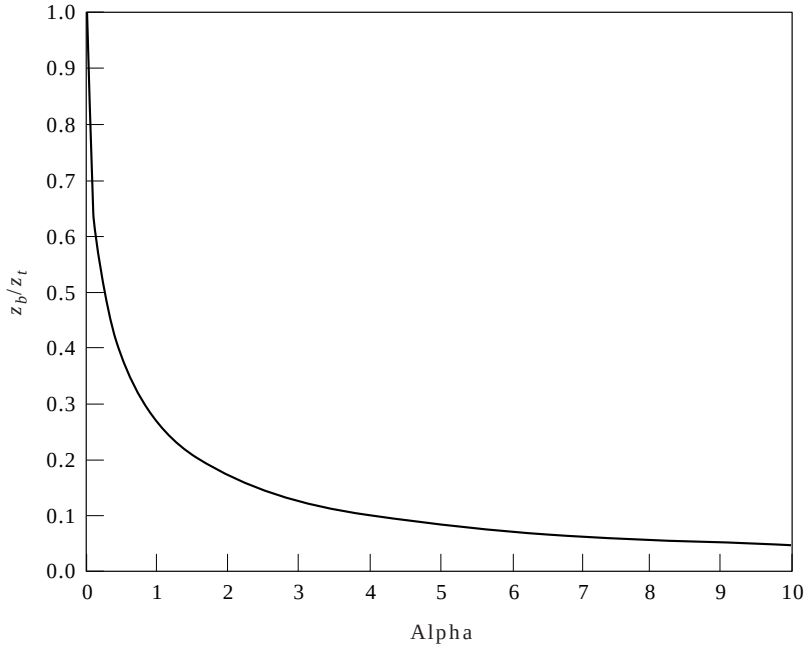

Figure 4. Normalized on-axis boundary z_b/z_t for $\alpha = 2T/\zeta$.

The behavior and sensitivity of z_b/z_t as a function of the parameter $2T/\zeta$ is shown in Figure 4.

The special case of $\zeta = 0$ which corresponds to the usual piston problem provides a useful baseline and is also readily addressed via the use of equations (33) and (34). It is noted that the on-axis pressure for this case has been previously addressed using an impulse response approach [14] and is simply expressed as follows for all T:

$$p_\sigma(0, z, \tau) = w(\tau - z) - w(\tau - \sqrt{1 + z^2}). \tag{39}$$

The first term in equation (39) corresponds to the field generated by an infinite planar aperture with a uniform velocity $w(\tau)$ and the latter term corresponds to the edge wave. In contrast to the case of $\zeta \neq 0$, the initial wave is not supersonic in nature.

For the case of a weighting function with a short pulse duration $2T$, it is apparent that two separate pulses will be observed over the range where $\Delta\tau \equiv \sqrt{1+z^2} - z > 2T$. The condition $\Delta\tau = \sqrt{1+z_{b0}^2} - z_{b0} = 2T$ defines a spatial boundary z_{b0} for the uniform piston case which is readily expressed as

$$z_{b0} = \frac{1 - (2T)^2}{2(2T)}, \zeta = 0. \tag{40}$$

It is also noted that the transition distance z_t is a maximum for this case, i.e., $z_t = \infty$.

If $\Delta\tau < 2T$ it is apparent that the individual pulses overlap in time and $p_\sigma(0, z, \tau)$ versus τ consists of three sections: an initial transient consisting of a finite section of $w(\tau - z)$, the overlapping section and a final transient consisting of a finite section of $w(\tau - \sqrt{1+z^2})$. Furthermore, if $\Delta\tau \ll 2\pi/\Omega_b = T_b$ it then follows from equation (39) that $p_\sigma(0, z, \tau)$ can be expressed as

$$p_\sigma(0, z, \tau) \approx \frac{w'(\tau - z)}{2z}, \tag{41}$$

where $w'(\tau)$ denotes the time derivative of $w(\tau)$. It is clear from the inverse range dependence that the asymptotic expression in equation (41) is a farfield result.

The minimum range of applicability in equation (41) is not unexpectedly linked to frequency via the condition that the time duration of the impulse response, i.e., the relative time delay between the pulses represented by the two terms in equation (39), is small relative to a time scale of interest which is taken here to be the period of the fundamental frequency Ω_b equation (20). For $z \gg 1$ it is noted that the relative time delay is then simply expressed as

$$\Delta\tau/T_b = 1/(2zT_b). \tag{42}$$

If the following condition is used to define the near/farfield transition distance z_{ff}:

$$\Delta\tau = T_b/4 = \pi/(2\Omega_b), \tag{43}$$

then z_{ff} can be expressed as

$$z_{ff} = \Omega_b/\pi, \tag{44}$$

which is the usual Rayleigh distance for a piston source. Clearly, z_{ff} can be expected to provide a reasonable estimate for the near- to farfield transition for pulsed fields associated with equation (20) for piston sources with large N. For small N, a larger value may be more appropriate to account for the higher frequencies in the spectrum, as noted in Figure 2.

Several measures may now be introduced in order to compare the performance of an aperture used to generate an acoustic BB to its performance with a uniform aperture distribution. An obvious measure is thus the normalized spatial boundary ratio z_b/z_{b0} which is readily expressed using equations (37) and (40) as a function of $2T$ and ζ, i.e.,

$$z_b/z_{b0} = \frac{2(2T)}{1-(2T)^2} \frac{\cos\zeta(\sin\zeta + 2T) - \sqrt{(2T)^2 + 2T\sin\zeta}}{\sin^2\zeta} \tag{45}$$

for $2T < 1 - \sin\zeta$. It is noted that the measure of performance is based solely on the separation of the edge wave from the initial wave. The results in Figure 5 illustrate that: the ratio $z_b/z_{b0} \leqslant 1$ for all T and ζ, the equality is satisfied only at $\zeta = 0$ for $2T < 1$ and $z_b/z_{b0} \to 0$ as $T \to 0$ for all $\zeta \neq 0$.

In order to discuss the near- to farfield transition distance for an acoustic BB with $\zeta \neq 0$ the importance of the transition distance z_t is first noted. As previously observed, z_t is the on-axis distance at which the initial wave and edge

wave intersect, i.e., $\Delta\tau = 0$. In light of the piston case, the transition distance z_t can thus be interpreted as the near- to farfield transition distance for acoustic BBs as $\Omega_b \to \infty$. This interpretation is useful since it is consistent with the usual definition of the Rayleigh distance for the piston case, i.e., it is apparent from equation (44) that $z_{ff} \to \infty$ as $\Omega_b \to \infty$ for which is the limiting result for z_t. Since the near- to farfield transition distance for an acoustic bullet must be less than z_t for any finite Ω_b, it is then apparent that there must be a minimum frequency above which the uniform aperture exhibits a larger near- to farfield transition distance than for an acoustic BB with $\zeta \neq 0$.

It is now apparent that an alternative measure of performance for acoustic BB fields is the ratio of the near- to farfield Rayleigh distance z_{ff} for a uniform aperture to the transition distance z_t which is independent of frequency, i.e.,

$$\frac{z_{ff}}{z_t} = \frac{\Omega_b \tan\zeta}{\pi}. \tag{46}$$

It then follows that the near- to farfield transition distance for a uniform aperture will be greater than or equal to that of an acoustic BB for a non-zero ζ providing

$$\Omega_b \geqslant \Omega_b^{\min} = \frac{\pi}{\tan\zeta}. \tag{47}$$

In retrospect, this result is not surprising since the Rayleigh distance for the uniform aperture increases with Ω_b whereas the frequency dependent near- to farfield transition distance for an acoustic BB for a non-zero ζ is bounded from above by a constant z_t.

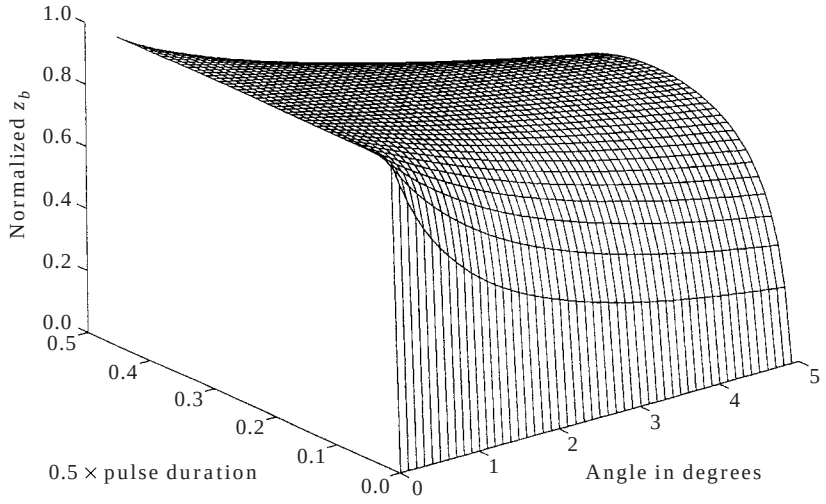

Figure 5. z_b/z_{b0} as a function of T and ζ.

A final measure to compare the performance of an acoustic BB to the field from a uniform aperture distribution is to recall that the near/far field transition distance z_{ff} for the uniform aperture was based on the condition $\Delta\tau = T_b/4$ in equation (43). If the same condition is now used for all ζ, it then follows that

$$\sqrt{1+z_f^2} - \sin\zeta - z_f\cos\zeta = \pi/(2\Omega_b). \tag{48}$$

For $\zeta = 0$ it is noted that

$$z_{f0} = \frac{1-[\pi/(2\Omega_b)]^2}{\pi/(\Omega_b)} \tag{49}$$

and $z_f \to z_{ff}$ as $\pi/(\Omega_b) \to 0$. More generally, it is easily shown that

$$\frac{z_f}{z_{f0}} = \frac{\pi/\Omega_b}{1-[\pi/(2\Omega_b)]^2}\frac{\alpha\cos\zeta - \sqrt{\alpha^2-(1-\alpha^2)\sin^2\zeta}}{\sin^2\zeta}, \tag{50}$$

where $\alpha \equiv [\sin\zeta + \pi/(2\Omega_b)]$.

Numerical results for z_f/z_{f0} versus ζ are presented in Figure 6 for $\Omega_b = 2^m\pi$ with $m = 1, 2, 3, 4$ and 5. For a fixed frequency Ω_b, the results show that z_f/z_{f0} is a monotonically decreasing function of ζ with a maximum at $\zeta = 0$. The minimum value of $z_f/z_{f0} = 0$ occurs when $\alpha = 1/\sqrt{2}$ or when $\sin\zeta = 1/\sqrt{2} - \pi/(2\Omega_b)$. In light of the results it thus appears that the near- to farfield transition distance for an acoustic BB with $\zeta \neq 0$ is less than the near-to farfield transition distance for the uniform aperture. Although the near- to farfield axial transition distance of the acoustic BB with $\zeta \neq 0$ may be less than the near-to farfield transition distance for the piston case where $\zeta \neq 0$, it is noted that the lateral or radial extent of the acoustic BB may also be less than the aperture size. The relative trade-off between axial range and lateral resolution is presently being investigated and the results will be reported in a later paper.

Although the short pulse case where $2T \ll 1$ is of primary interest here, it is worthwhile to conclude this subsection by addressing the long pulse case where $2T \gg 1$ and $N \gg 1$ for the finite planar aperture. After introducing the following Fourier transform pairs

$$h_\sigma(\rho, z, \tau) \Leftrightarrow H_\sigma(\rho, z, \Omega), \quad p_\sigma(\rho, z, \tau) \Leftrightarrow P_\sigma(\rho, z, \Omega), \tag{51, 52}$$

it then follows from equations (7) and (8) that

$$P_\sigma(\rho, z, \Omega) = i\Omega W(\Omega) H_\sigma(\rho, z, \Omega), \tag{53}$$

where

$$H_\sigma(\rho,z,\Omega) = \cos\zeta \int_0^\sigma \rho_s \, \mathrm{d}\rho_s \int_0^{2\pi} \mathrm{d}\phi_s \frac{\mathrm{e}^{-i\Omega R}}{2\pi R} J_0(\Omega \sin\zeta \rho_s). \tag{54}$$

It is noted that equation (54) is equivalent to the usual Rayleigh surface integral representation for a harmonic field.

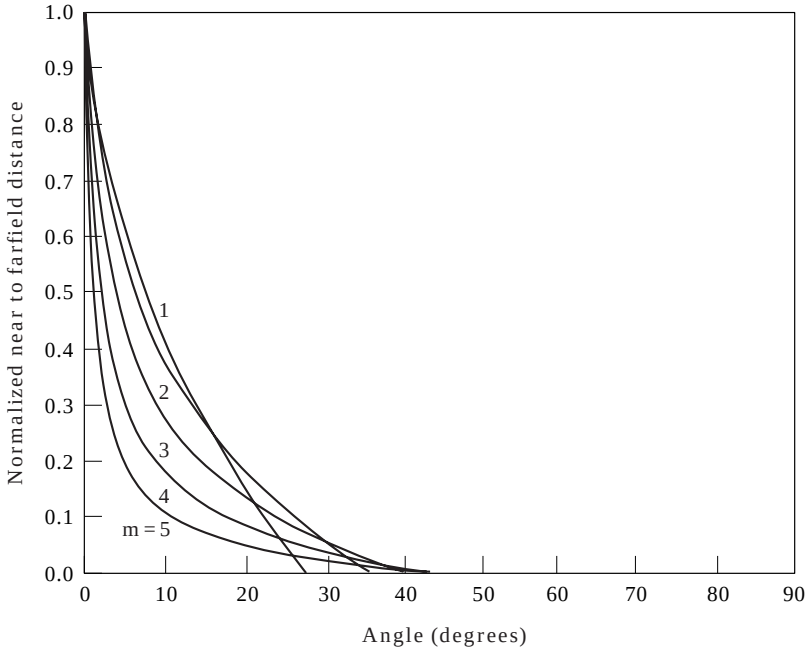

Figure 6. z_f/z_{f0} versus ζ for $\Omega_b = 2^m\pi$ with $m = 1, 2, 3, 4$ and 5.

Now for $N \gg 1$ it is then easily shown that the steady state component of the pressure field (neglecting the turn-on and turn-off transients) can be simply expressed as

$$p_\sigma(\rho, z, \tau) = \mathrm{Re}\{i\Omega_b H_\sigma(\rho, z, \Omega_b)\mathrm{e}^{i\Omega_b\tau}\}. \tag{55}$$

For the on-axis case it is then apparent from equation (54) that

$$\begin{aligned} H_\sigma(0, z, \Omega_b) &= \cos\zeta \int_0^\sigma \rho_s \, \mathrm{d}\rho_s \frac{\mathrm{e}^{-i\Omega_b\sqrt{z^2+\rho_s^2}}}{\sqrt{z^2+\rho_s^2}} J_0(\Omega_b \sin\zeta\rho_s) \\ &= \cos\zeta \, \mathrm{e}^{-i\Omega_b z} \int_0^\alpha J_0(\Omega_b \sin\zeta\sqrt{y^2+2zy}) \, \mathrm{e}^{-i\Omega_b y} \, \mathrm{d}y, \end{aligned} \tag{56}$$

where $\alpha = \sqrt{z^2+1} - z$. The farfield pressure may also be simply obtained and can be expressed as

$$p_\sigma^f(R_0, \theta, \tau) = \mathrm{Re}\{i\Omega_b H_\sigma^f(R_0, \theta, \Omega_b) \, \mathrm{e}^{i\Omega_b\tau}\}, \tag{57}$$

where

$$H_\sigma^f(R_0, \theta, \Omega_b) = \frac{\mathrm{e}^{-i\Omega_b R_0}}{2\pi R_0} \pi\sigma^2 \cos\zeta G_\sigma(\theta, \zeta, \Omega_b) \tag{58}$$

and

$$G_\sigma(\theta, \zeta, \Omega_b) \equiv \frac{1}{[\sin^2\zeta - \sin^2\theta]}\left[\sin^2\zeta J_0(\Omega_b\sigma\sin\theta)\frac{2J_1(\Omega_b\sigma\sin\zeta)}{\Omega_b\sigma\sin\zeta}\right.$$
$$\left. - \sin^2\theta J_0(\Omega_b\sigma\sin\zeta)\frac{2J_1(\Omega_b\sigma\sin\theta)}{\Omega_b\sigma\sin\theta}\right]. \quad (59)$$

For $\theta = 0$ it is noted that

$$G_\sigma(0, \zeta, \Omega_b) = \frac{2J_1(\Omega_b\sigma\sin\zeta)}{\Omega_b\sigma\sin\zeta}. \quad (60)$$

4. NUMERICAL RESULTS

In contrast to the preceding section, numerical results are now presented to illustrate the characteristics of the acoustic BB fields for some specific cases of interest. The results are presented first for the case of an infinite aperture and then for the case of a finite aperture. Analogous numerical results for the pressure time histories for a uniformly excited aperture are presented for the finite aperture in order to provide a baseline for comparison.

Consider first the case of an infinite aperture where $\Omega_b = 20$ and $2N = 10$. A pressure map for $p(\rho, 0, \tau)$ is shown in Figure 7 as a function of normalized time τ and normalized radial distance $\rho_r = \rho\sin\zeta$ for $0 \leqslant \rho_r \leqslant 0{\cdot}5$. The results clearly illustrate the expected space–time dependence of $p(\rho, 0, \tau)$. Since $T > \rho_r = \rho\sin\zeta$ over the indicated range of ρ_r, the turn-on and turn-off transients are relatively minor contributors to the overall time responses which are controlled by the quasi steady state pressure contribution. It is noted that the quasi steady state results are in agreement with the analytical result in equation (31) and the on-axis pressure $p(0, 0, \tau)$ corresponds to $w(\tau)$. The lateral extent of the acoustic BB is also noted to be in agreement with equation (32) and the on-axis axial extent of the acoustic BB is determined by $2T$.

In contrast to the preceding quasi-steady state example for the case of an infinite aperture, a pressure map for $p(\rho, 0, \tau)$ where $\Omega_b = 20$ and $2N = 2$ is shown in Figure 8 as a function of normalized time τ and normalized radial distance ρ_r. A similar result is also shown in Figure 9 for the case of $2N = 1$, i.e., a single cycle of the excitation corresponding to $w_0 = -1$ in equation (20). As a result of the shorter pulse durations, the turn-on and turn-off transients are of greater importance relative to the quasi steady state pressure contribution which only exists in the region where $0 \leqslant \rho_r \leqslant T$. Equation (32) again provides a reasonable estimate of the lateral extent of the acoustic BB and the axial extent is again determined by the pulse duration $2T$. The on-axis pressure $p(0, 0, \tau)$ again corresponds to $w(\tau)$. In the region where $\rho_r > T$, two distorted quasi-sinusoidal signals are readily observed in the pressure time history at each point, and in general the spectral content of the signals decreases as ρ_r increases.

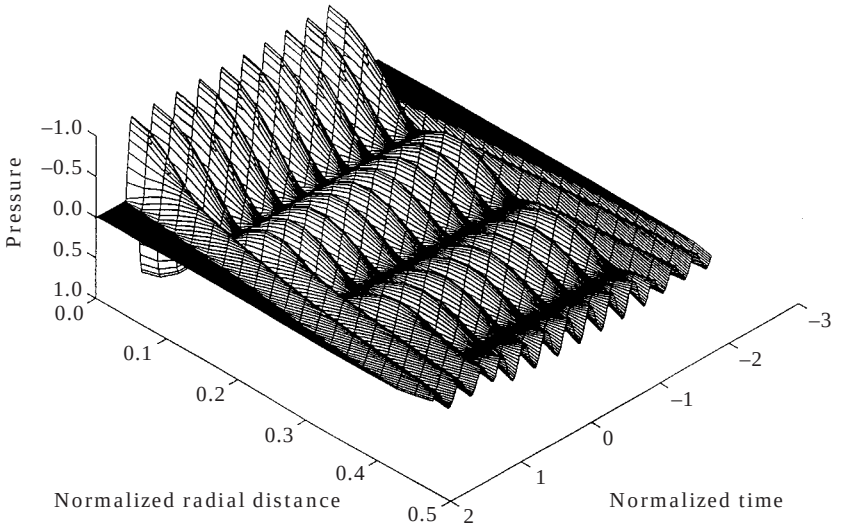

Figure 7. Space–time pressure about the pulse center for $\Omega_b = 20$ and $2N = 10$.

Consider now the case of a finite aperture where $\sigma = 1$ and the gated sinusoidal weighting function $w(\tau)$ in equation (20) is again used as the excitation where $\Omega_b = 45$, $2N = 1$ and $w_0 = -1$ for the first case of interest. On-axis pressures $p(0, z, \tau)$ are presented in Figure 10 as a function of a normalized time $(\tau - z)$ for $z/z_t = 0$, 1/4, 1/2, 1, 2 and 4. Numerical results in each figure are presented for two cases: $\zeta = \pi/6$ and 0, i.e., the latter being the piston case. It is noted that the transition distance is $z_t = \sqrt{3}$ for the case of $\zeta = \pi/6$ and the Rayleigh distance is $z_{ff} = 14{\cdot}3$ for the piston case.

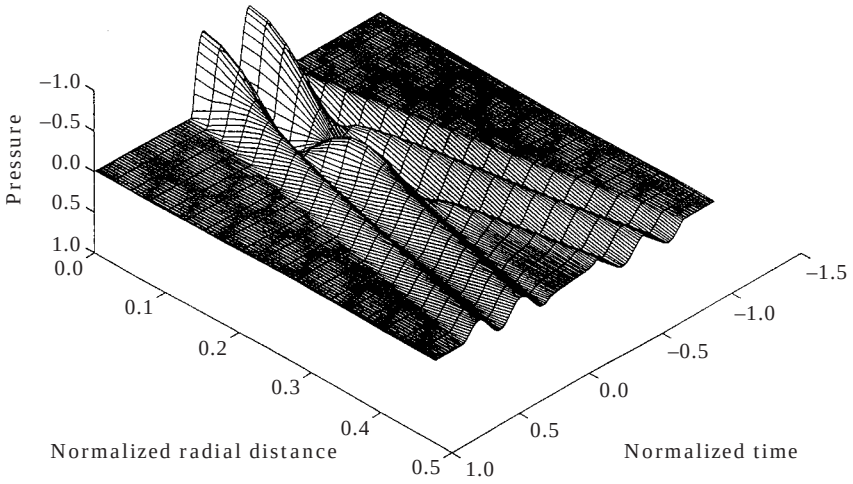

Figure 8. Space–time pressure about the pulse center for $\Omega_b = 20$ and $2N = 2$.

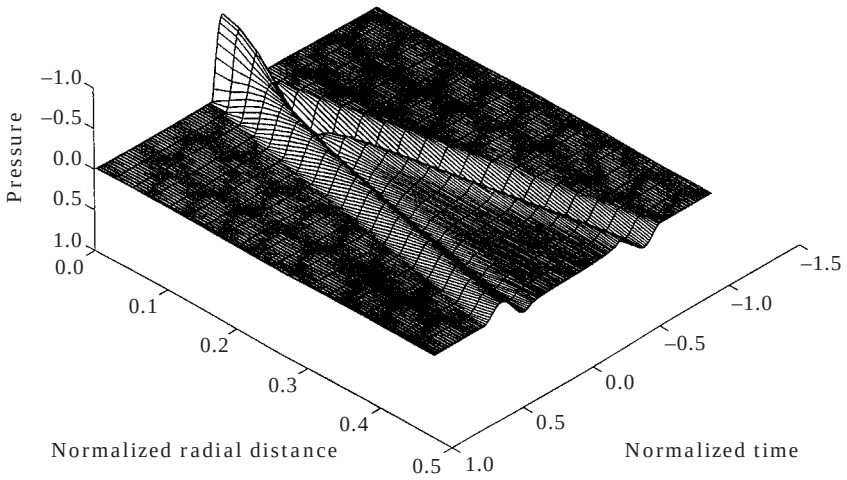

Figure 9. Space–time pressure about the pulse center for $\Omega_b = 20$ and $2N = 1$.

First, several observations of interest for the piston case are readily apparent from the numerical results in Figure 10. The plane wave and edge components of the pressure are clearly separated in time for the piston case when $z/z_t < 2$. In the region where $2 < z/z_t < 8$ the plane and edge wave components are noted to overlap, thus resulting in an interference pattern in time. The peak value of the field for points in this axial region varies between 1 and 2 up to $z/z_t = 8$ which is approximately the Rayleigh distance based on Ω_b.

Several important observations regarding the acoustic BB are also apparent from Figure 10. As expected, the numerical result for the acoustic BB pressure at $z/z_t = 0$ is noted to consist of two components: a direct wave component which is identical to the plane wave result for the piston case and an edge wave component which is significantly reduced in amplitude with a longer time duration than the piston case. The latter features are characteristic of the edge wave for all axial distances. For $z/z_t = 1/2$ it is clearly noted that the initial pressure for the acoustic BB field arrives prior to the initial plane wave contribution for the piston, i.e., the on-axis field propagates at a supersonic speed ($1/\cos\zeta = 2/\sqrt{3}$). The edge wave for this axial distance overlaps the initial direct wave for the BB field. However, the most remarkable feature of the acoustic BB field is the significant reduction in the amplitude of the field in the region $z/z_t \approx 1$. In this region the acoustic BB field exhibits a more rapid decay with distance than the ubiquitous inverse range law.

Consider again the case of a finite aperture where $\sigma = 1$ and the gated sinusoidal weighting function $w(\tau)$ with $\Omega_b = 45$, $2N = 1$ and $w_0 = -1$; however, the angle ζ is now reduced by a factor of 10, i.e., $\zeta = \pi/60$. It is noted that the transition distance is $z_t = 19{\cdot}08$ for the case of $\zeta = \pi/60$ and the Rayleigh distance is unchanged, i.e., $z_{ff} = 14{\cdot}3$ for the piston case. On-axis pressures $p(0, z, \tau)$ are presented in Figure 11 as a function of a normalized time relative

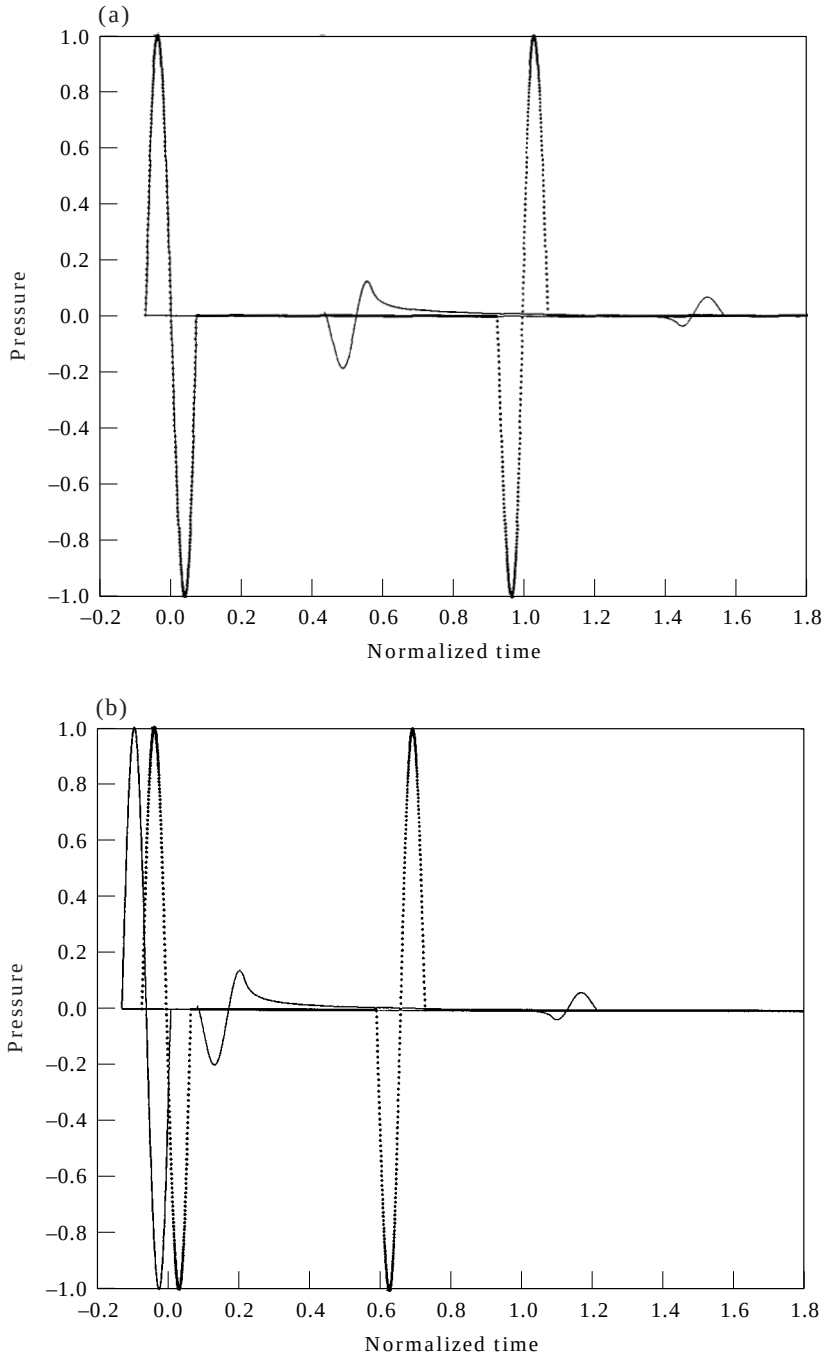

Fig. 10. (*Caption on p.* 134)

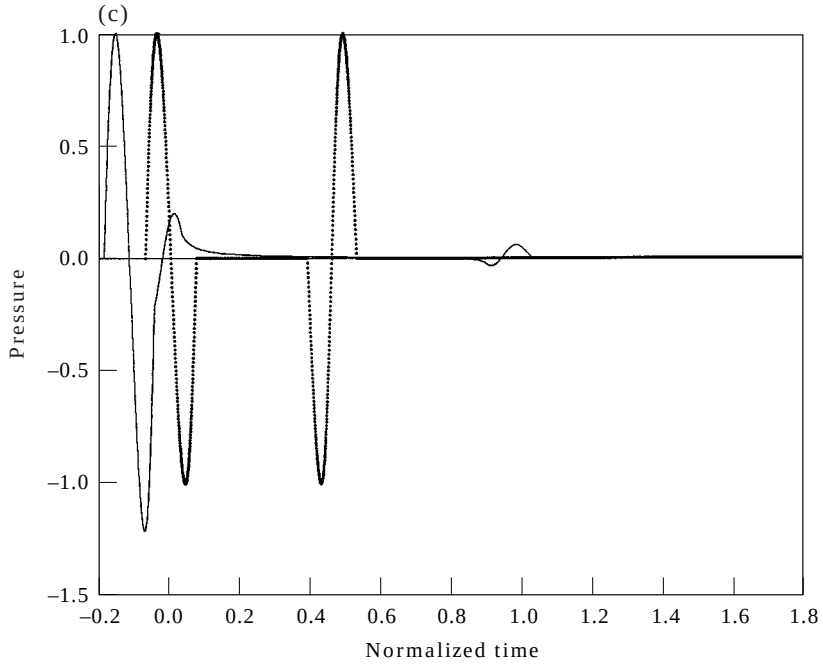

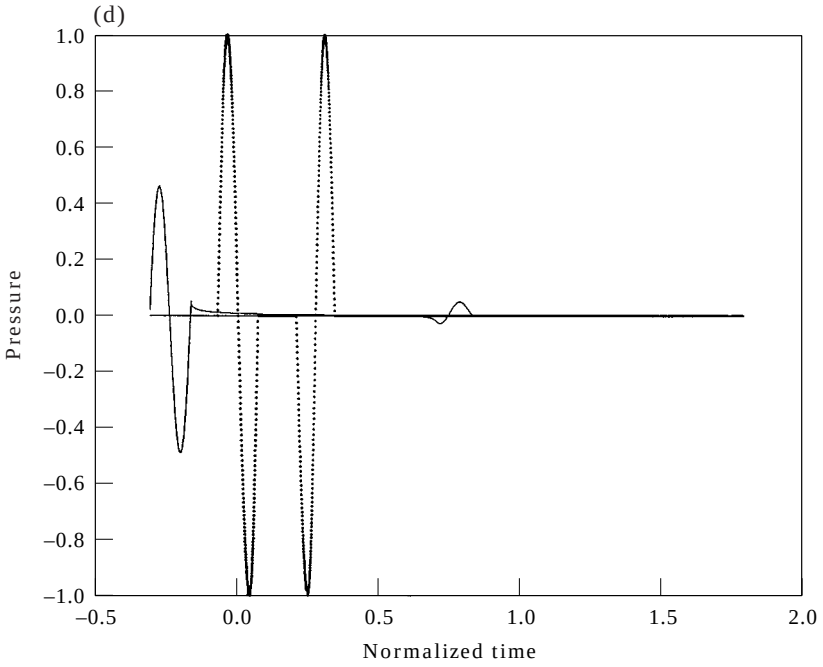

Fig. 10. (*Caption on p.* 134)

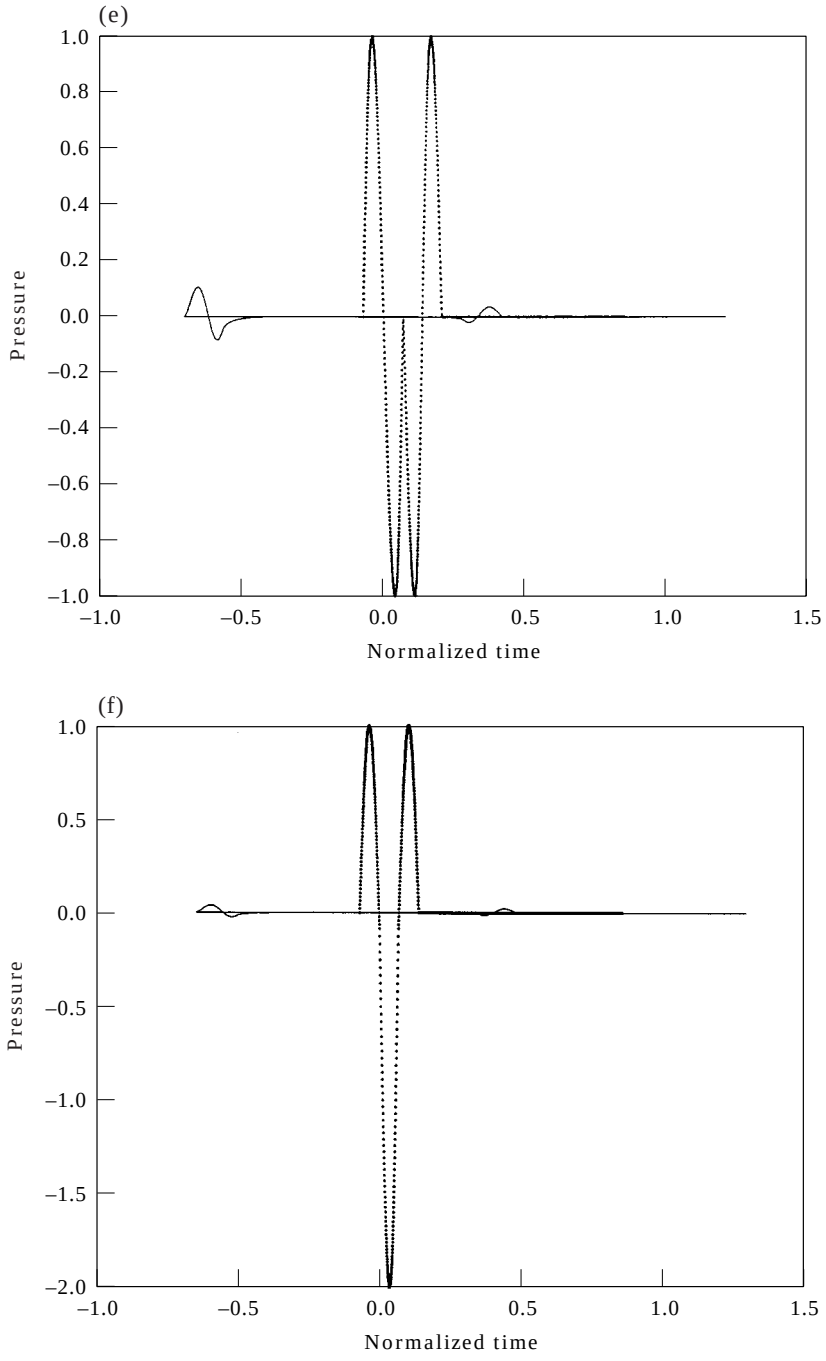

Figure 10. Pressure versus normalized time for $\Omega_b = 20$ and $2N = 1$ for piston case (. . . . . .) and acoustic bullet with $\zeta = 30°$: (a) $z/z_t = 0$; (b) $z/z_t = 1/4$; (c) $z/z_t = 1/2$; (d) $z/z_t = 1$; (e) $z/z_t = 2$; (f) $z/z_t = 4$.

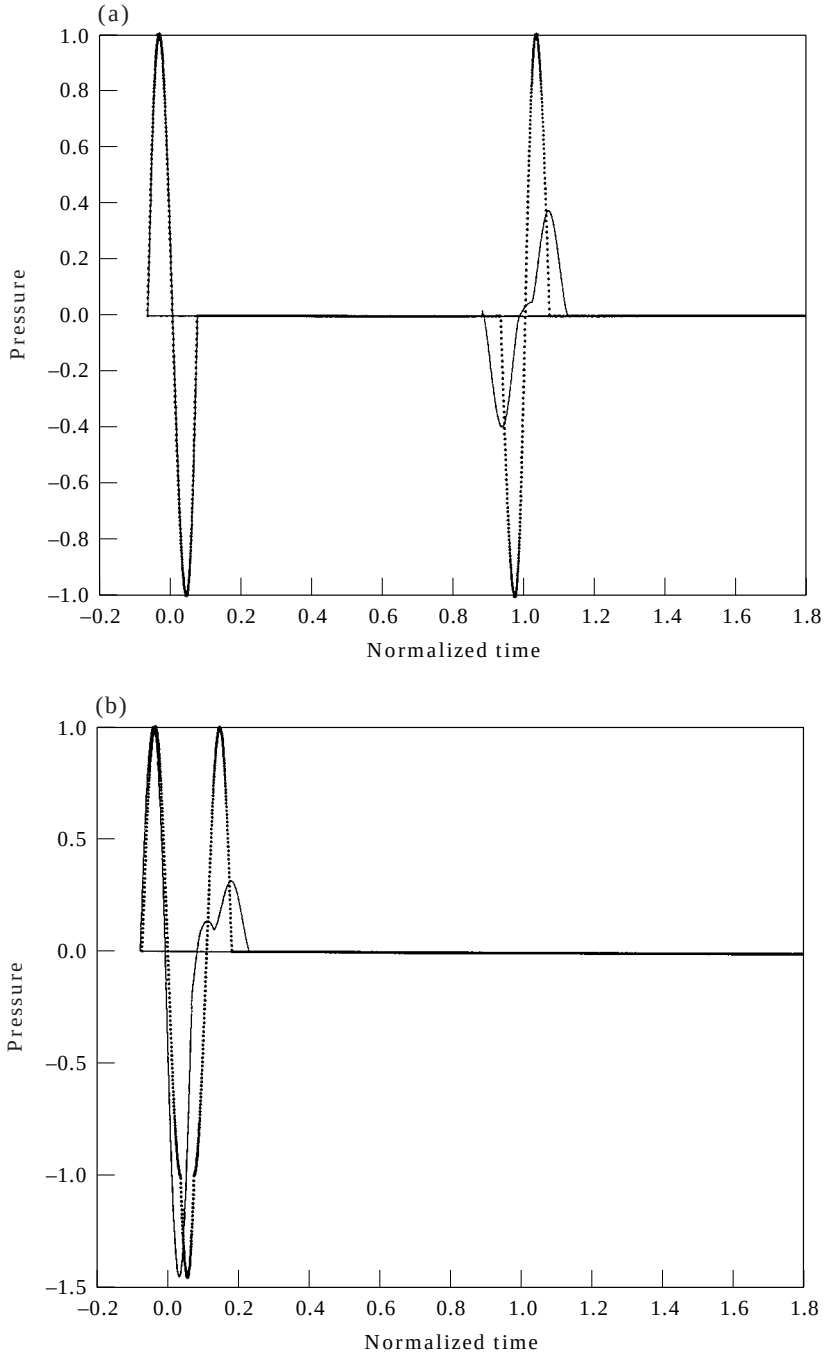

Fig. 11. (*Caption on p.* 137)

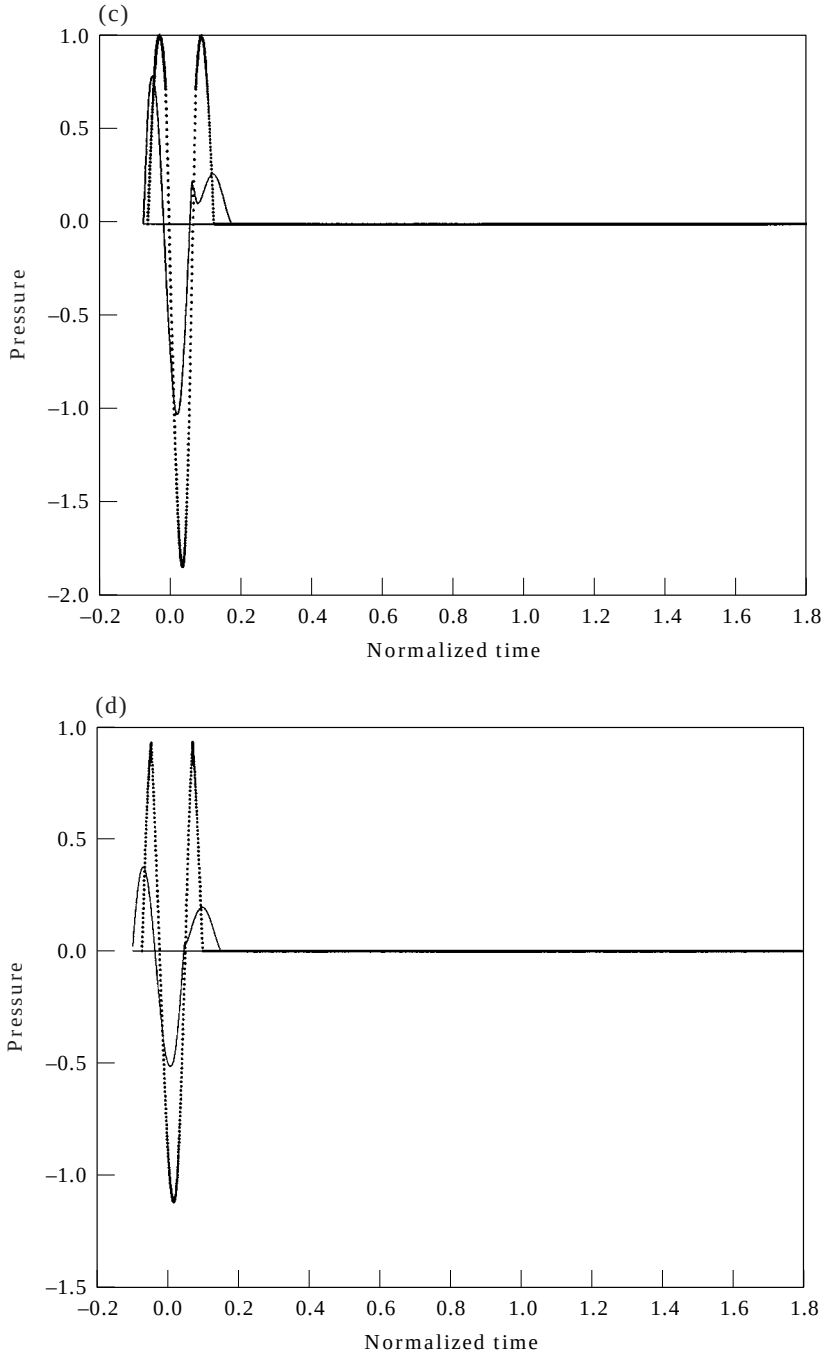

Fig. 11. (*Caption on p.* 137)

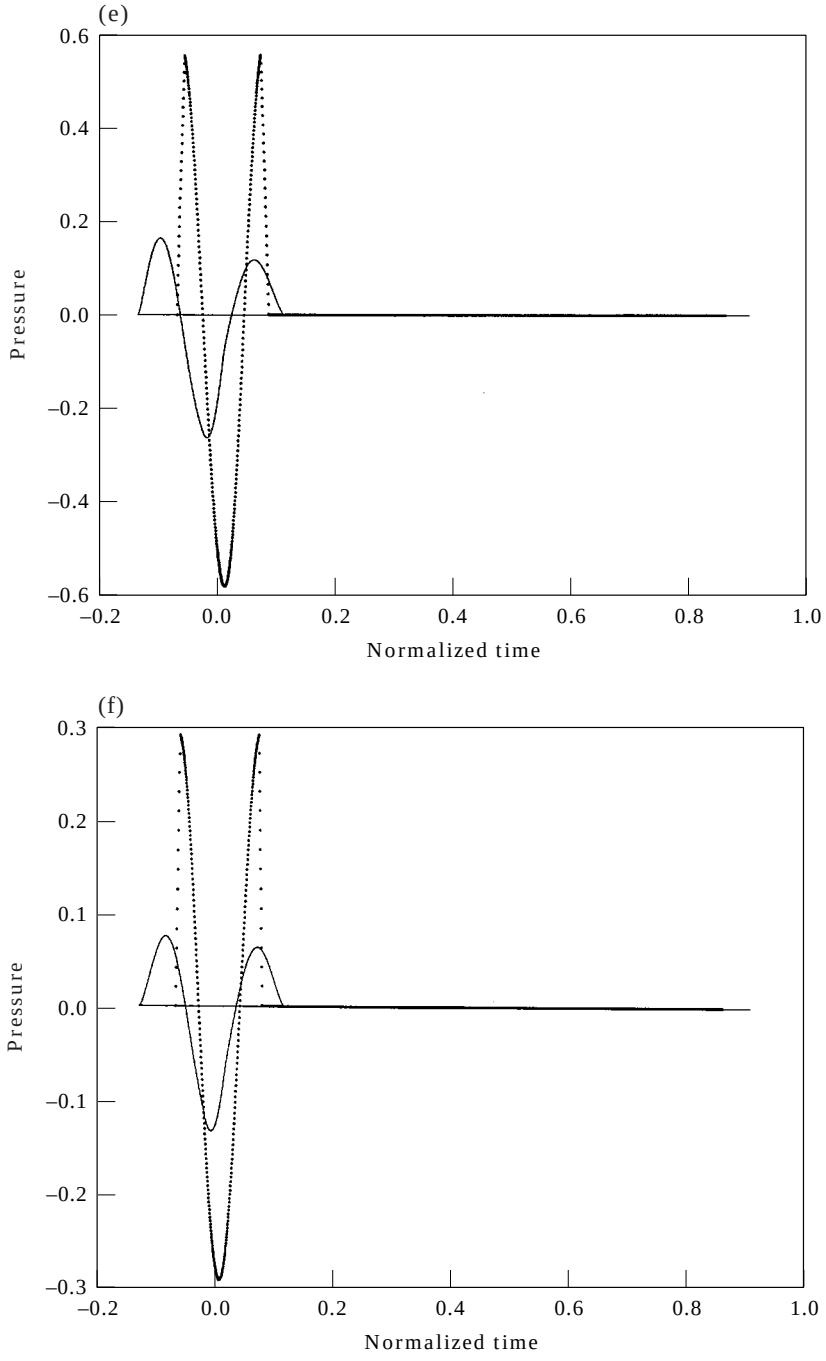

Figure 11. Pressure versus normalized time for $\Omega_b = 20$ and $2N = 1$ for piston case (. . . . . .) and acoustic bullet with $\zeta = 3°$: (a) $z/z_t = 0$; (b) $z/z_t = 1/4$; (c) $z/z_t = 1/2$; (d) $z/z_t = 1$; (e) $z/z_t = 2$; (f) $z/z_t = 4$.

to $\tau = z$ for $z/z_t = 0$, 1/4, 1/2, 1, 2 and 4. A comparison of the acoustic BB results in Figures 10 and 11 illustrates the relative importance of the edge waves for $\zeta = \pi/6$ and $\pi/60$. Clearly the edge waves are more comparable in amplitude to those of the piston case as $\zeta \to 0$. This result is of course to be expected since the piston case corresponds to $\zeta = 0$.

As a final case of interest consider now a finite aperture and gated sinusoidal excitation where $\sigma = 1$ and $\zeta = \pi/60$ and 0. The frequency of excitation is now selected to be $\Omega_b = 73{\cdot}18$ which results in an on-axis farfield null for the steady state pressure as noted from equation (60), i.e., $J_1(\Omega_b \sin \zeta) = 0$ for the $\zeta = \pi/60$ case. On-axis pressures $p(0, z, \tau)$ are presented in Figure 12 for $2N = 4$ as a function of a normalized time relative to $\tau = z$ for $z/z_t = 1$, 2, 4, 8 and 16. On-axis normalized energy plots for the $\zeta = \pi/60$ and piston cases are presented in Figure 13 as a function of the normalized axial distance z/z_t. The normalized energy ratio at each point is defined to be the integral of the squared pressure divided by the integral of the squared weighting function, i.e., T.

The results in Figure 12 clearly show a significant change in the nature of the on-axis pressure as z/z_t increases. In particular, the importance of the edge contributions of the edge wave increase as z/z_t increases for the $\zeta = \pi/60$ case. For $z/z_t \gg 1$ the edge contributions corresponding to the turn-on and turn-of transients exhibit an inverse range dependence whereas the corresponding steady state portion of each pressure must decay at a faster rate (recall $J_1(\Omega_b \sin \zeta) = 0$). A clearer picture of this spatial decay process is shown in Figure 13 for the energy plot. In this figure the normalized energy for the $\zeta = \pi/60$ case is seen to exhibit a sharp dropoff from its nearfield level when $z/z_t \approx 1$. This near- to farfield transition results in a rapid spatial rolloff of the energy which is subsequently followed by the farfield region where the energy decays inversely with the square of the range.

A simple explanation for the general characteristics of the spatial decay of the on-axis energy field is readily obtained from the solution of the analogous harmonic problem in which the pulse duration of interest is considered to be long enough so that $W(\Omega)$ is spectrally pure. Numerical results for the normalized intensity of the pressure as a function of z/z_t are presented in Figure 14 for the preceding $\zeta = \pi/60$ and piston cases for $\Omega_b = 73{\cdot}18$. As expected the intensity for the piston case exhibits an inverse square dependence on range whereas the intensity for the $\zeta = \pi/60$ case exhibits a much faster rolloff. An additional result for the normalized intensity corresponding to the $\zeta = \pi/60$ case is also presented for $\Omega_b = 103{\cdot}6$. This result shows that the field for this frequency clearly exhibits an inverse square dependence on range. It is thus apparent that the inverse square dependence on range for the on-axis energy for acoustic Bessel Bullets is associated with the spectral components of $W(\Omega)$ where $J_1(\Omega_b \sin \zeta) \neq 0$.

5. SUMMARY AND CONCLUSIONS

Acoustic Bessel Bullets are defined to be a class of Transient Bessel Beam (TBB) wavefields. An acoustic Bessel Bullet (BB) with a smaller support region

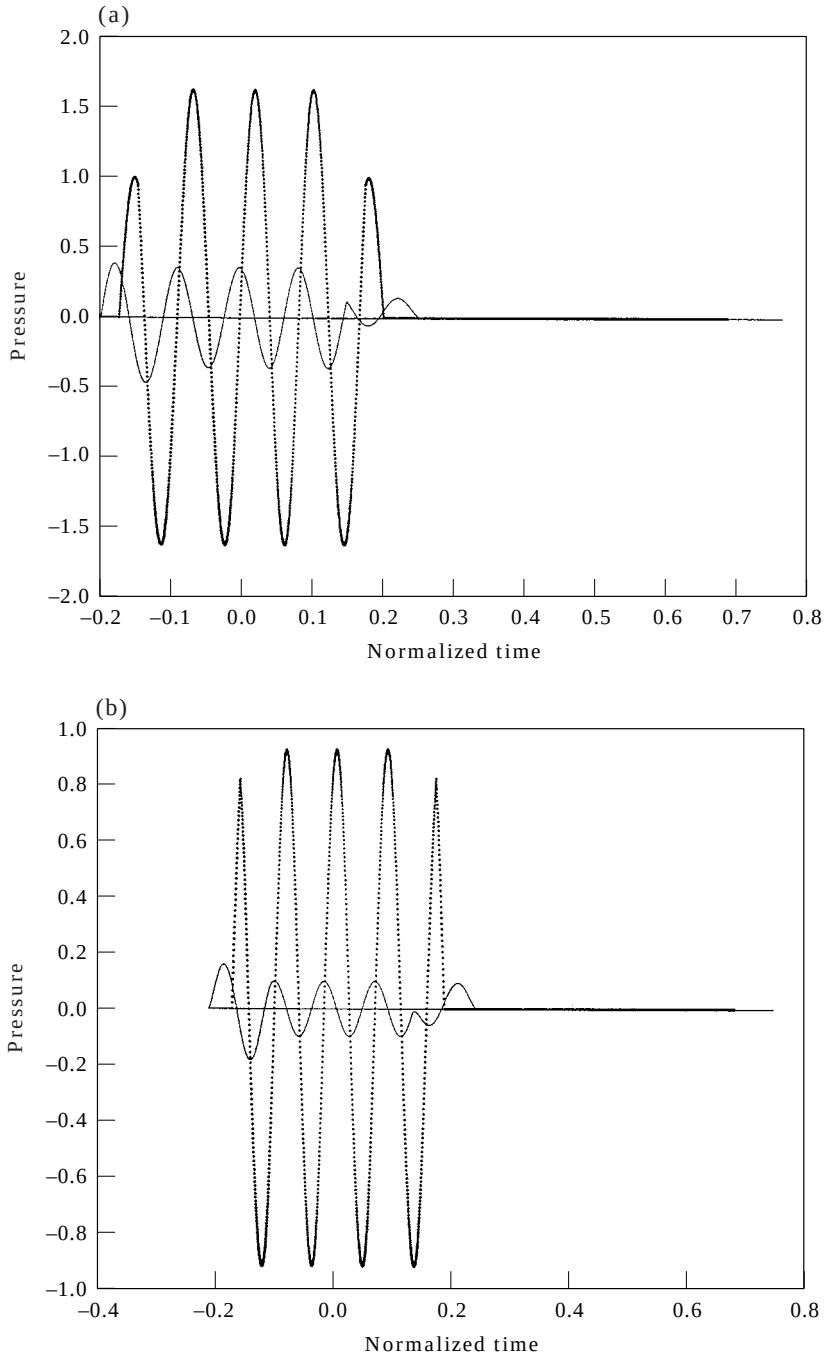

Fig. 12. (*Caption on p.* 141)

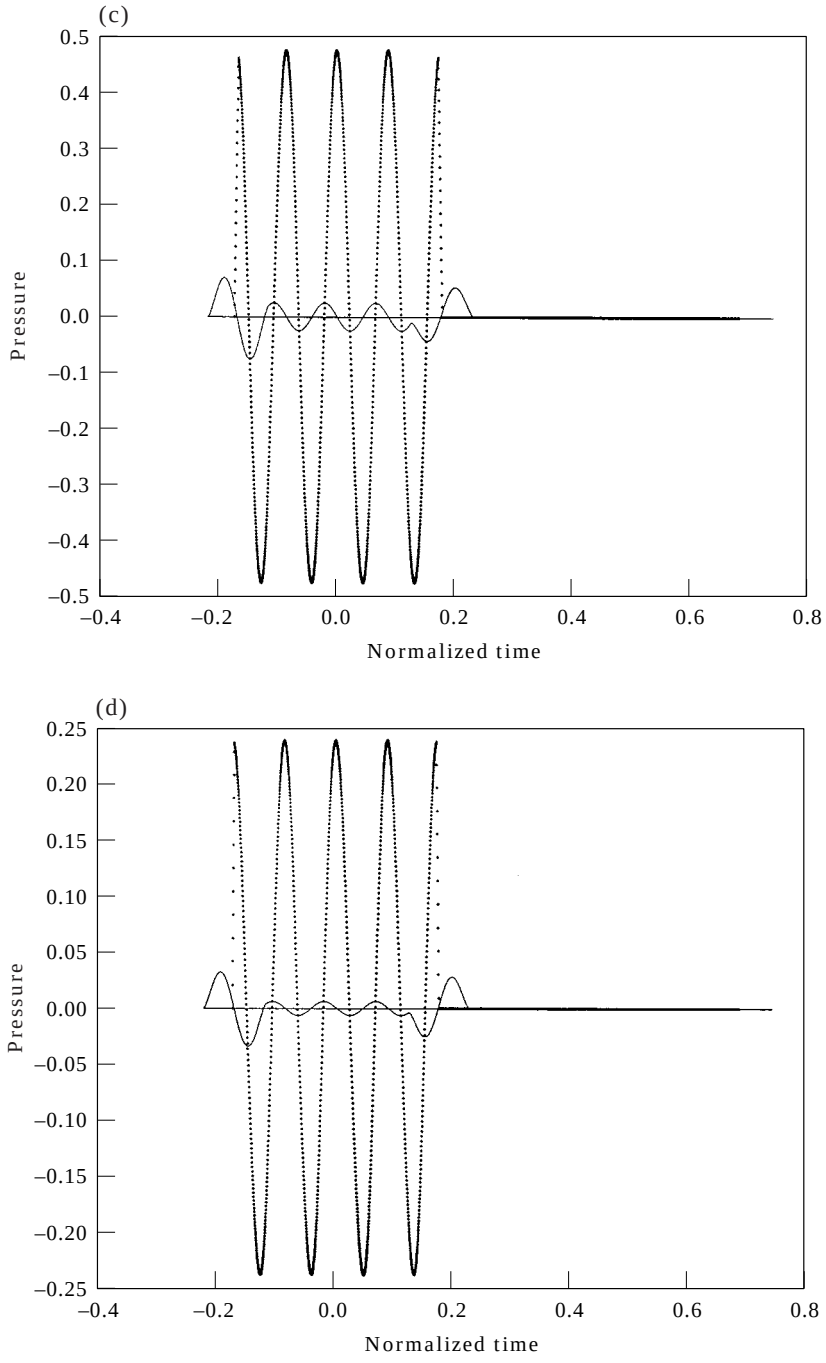

Fig. 12. (*Caption on p.* 141)

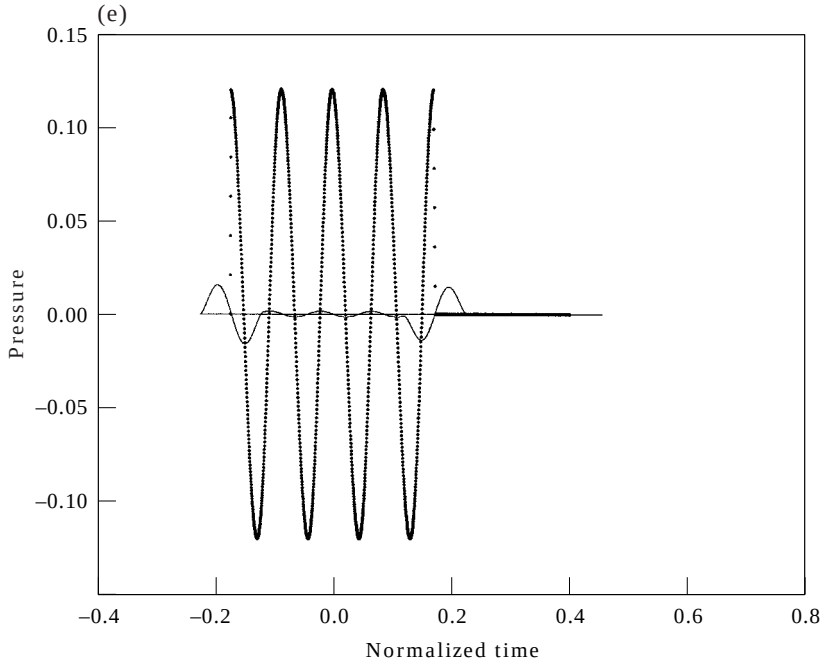

Figure 12. Pressure versus normalized time for $\Omega_b = 73{\cdot}18$ and $2N = 4$ for piston case (. . . . . .) and acoustic bullet with $\zeta = 3°$: (a) $z/z_t = 1$; (b) $z/z_t = 2$; (c) $z/z_t = 4$; (d) $z/z_t = 8$; (e) $z/z_t = 16$.

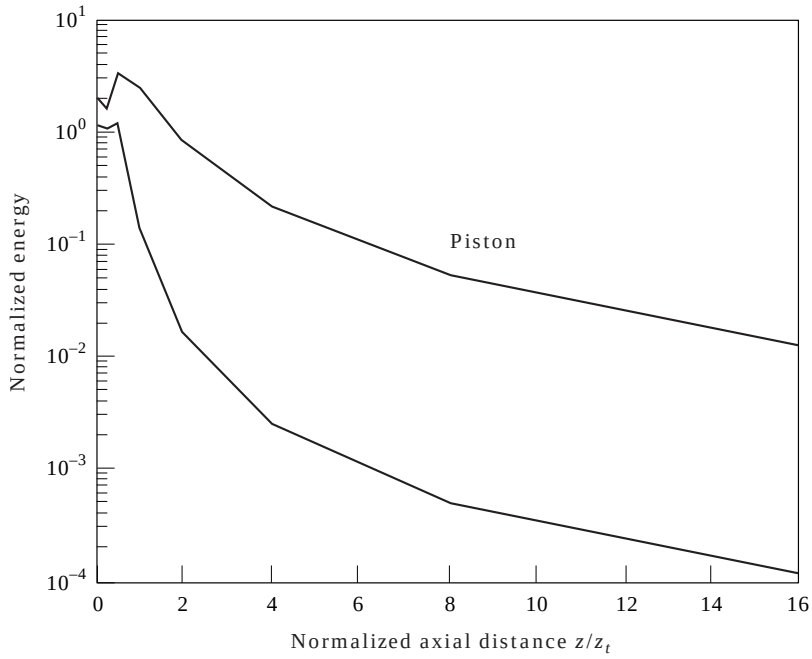

Figure 13. Normalized energy versus normalized axial distance z/z_t for piston case and acoustic bullet with $\zeta = 3°$.

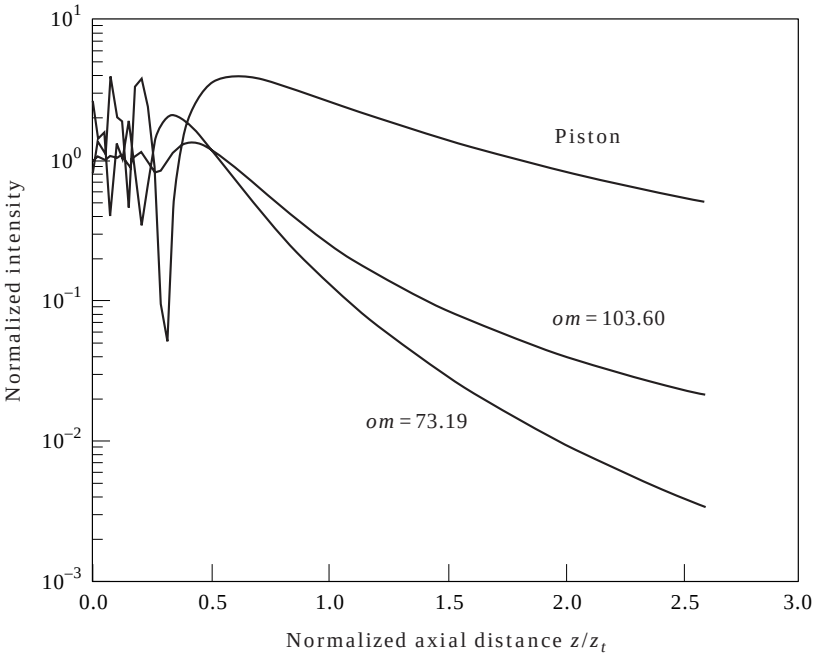

Figure 14. Normalized intensity versus normalized axial distance z/z_t for piston case and acoustic bullets where $\Omega_b = 73{\cdot}18$ and $\Omega_b = 103{\cdot}6$ with $\zeta = 3°$.

than a circular planar aperture can be launched from a finite aperture with a specified space–time normal acceleration distribution which is based on a pulsed sinusoidal signal. In a limited nearfield space–time region the acoustic BB field generated by a finite aperture exhibits properties similar to those observed for the infinite aperture case, and in the farfield region the field exhibits an inverse range dependence.

Analytical expressions for the on-axis and farfield for acoustic Bessel Bullets are developed for the infinite and finite aperture cases using a previously presented generalized impulse response approach. The expressions can be used to investigate the limitations and the space–time properties of the BB fields as a function of the center frequency and bandwidth or pulse length of the excitation. In particular, the expressions provide important information on the spatial and axial extent of acoustic Bessel Bullets. Expressions for the space–time field for a finite aperture with a spatially uniform distribution which is a special case of an acoustic bullet are also presented as a baseline for comparison.

Numerical results for the case of an infinite aperture are first presented to provide a baseline and to illustrate the effects of carrier frequency and pulse length on the axial and lateral extent and the general space–time properties of the acoustic BB field. The axial extent of the bullet is determined by the pulse length of the excitation whereas the radial extent is determined by the excitation frequency and the axicon angle ζ. Numerical results for the case of a finite

aperture are then presented to illustrate the general space–time properties of the on-axis field for acoustic BBs relative to the field generated from the aperture with a spatially uniform excitation. These results indicate that the largest near-to farfield transition distance occurs for the case of a uniform excitation. The Rayleigh distance for this latter case appears to provide an upper limit for the near field for acoustic BB fields. Although acoustic BB fields from finite apertures exhibit shorter transition distances relative to the uniform case, there is also a concomitant reduced lateral extent of the field which may be advantageous in certain applications.

REFERENCES

1. J. N. Brittingham 1983 *Journal of Applied Physics* **54**, 1179–1189. Focus wave modes in homogeneous Maxwell's equations: transverse electric mode.
2. R. W. Ziolkowski 1985 *Journal of Mathematical Physics* **26**, 861–863. Exact solutions of the wave equation with complex source locations.
3. R. W. Ziolkowski, I. M. Besieris and A. M. Shaarawi 1991 *Proceedings of IEEE* 79, 1371–1378. Localized wave representations of acoustic and electromagnetic radiation.
4. I. M. Besieris, A. M. Shaarawi and R. W. Ziolkowski 1989 *Journal of Mathematical Physics* **30**, 1254–1269. A bidirectional traveling plane wave representation of exact solutions of the scalar wave equation.
5. J. V. Candy, R. W. Ziolkowski and D. K. Lewis 1990 *Journal of Acoustical Society of America* **88**, 2235–2247. Transient waves estimation: a multichannel deconvolution application.
6. J. V. Candy, R. W. Ziolkowski and D. K. Lewis 1990 *Journal of Acoustical Society of America* **88**, 2248–2258. Transient waves: reconstruction and processing.
7. J. E. Hernandez, R. W. Ziolkowski and S. R. Parker 1992 *Journal of Acoustical Society of America* **92**, 550–562. Synthesis of the driving functions of an array for propagating localized wave energy.
8. T. T. Wu 1985 *Journal of Applied Physics* **57**, 2370–2373. Electromagnetic missiles.
9. T. T. Wu, R. W. P. King and H. M. Shen 1987 *Journal of Applied Physics* **62**, 4036–4040. Spherical lens as a launcher of electromagnetic missiles.
10. R. W. Ziolkowski and D. K. Lewis 1990 *Journal of Applied Physics* **68**, 6083–6086. Verification of the localized wave transmission effect.
11. R. W. Ziolkowski 1991 *Physics Review A* **44**, 3960–3984. Localized wave physics and engineering.
12. P. R. Stepanishen and J. Sun 1997 *Journal of Acoustical Society of Americ a* **102**, 1955–1963. Acoustic bullets: transient bessel beams generated by planar apertures.
13. P. R. Stepanishen 1998 *Journal of Acoustical Society of America* **103**, 1742–1751. Acoustic bullets/transient bessel beams: near to far field transition via an impulse response approach.
14. P. R. Stepanishen 1971 *Journal of Acoustical Society of America* **49**, 1629–1638. Transient radiation from pistons in an infinite planar baffle.